Supporting Information

Amplification factor in DC insulator-based electrokinetic devices: a theoretical, numerical, and experimental approach to operation voltage reduction for particle trapping

Rodrigo Ruz-Cuen,[1] J. Martin de los Santos-Ramírez,[1] Braulio Cardenas-Benitez,[3] Cinthia J. Ramírez-Murillo,[1] Abbi Miller,[2] Kel Hakim,[2] Blanca H. Lapizco-Encinas,[2] and Victor H. Perez-Gonzalez.[1,*]

[1] School of Engineering and Sciences, Tecnologico de Monterrey, NL 64849, Mexico

[2] Microscale Bioseparations Laboratory, Rochester Institute of Technology, Rochester NY 14623, USA

[3] Department of Biomedical Engineering, University of California, Irvine, Irvine, CA 92697, USA

*Corresponding author:

Dr. Victor H. Perez-Gonzalez, Email: vhpg@tec.mx

Contents

1 Analytical model for the nonuniform electric field

1.1 Electric field solution in elliptical coordinates

We begin by considering the geometry presented in Fig. 2d of the main Manuscript, which shows two dielectric interfaces demarcated by hyperbolas ($\nu =$ const.) in the elliptical system of coordinates (μ,ν). The space between the hyperbolas, considered to be the outside region (o), is filled with a dielectric material of permittivity ϵ_o and conductivity σ_o, while the region inside (i) dielectric posts has a permittivity

of ϵ_i and conductivity σ_i. For this configuration, the foci of hyperbolas lay in the x-axis, at coordinates $(a,0)$, and $(-a,0)$, and hyperbolas are separated a distance $G = 2a\cos\nu_0$. Our objective is to obtain the electric potential and the electric field inside the region of interest $0 \le \mu \le \mu_0$, $0 \le \nu < 2\pi$, which is chosen to approximate the two- triangle constriction geometry in the microfluidic channel.

As boundary condition, a DC voltage V_0 is applied at the μ_0 boundary outside of the inner dielectric, where $\nu_0 \le \nu \le \pi - \nu_0$, and a $-V_0$ voltage at the lower end, where $\mu = \mu_0$ and $\pi + \nu_0 \le \nu \le 2\pi - \nu_0$. These boundaries at $\mu = \mu_0$ are chosen to be separated exactly by a distance L along the y-axis, and thus one can define the relevant electric field magnitude $E_0 = 2V_0/L = \Delta V/L$ that approximates the experimental condition of applying an outer electric field $E_0\hat{j}$. There are two electric potentials that need to be determined inside the region of interest, corresponding to the potential inside the dielectric tips, ϕ_i, and the potential on the outside medium, ϕ_o. The symmetry of the problem requires that $\phi_k(\nu,\mu) = \phi_k(\pi - \nu,\mu)$, $\phi_k(\pi + \nu,\mu) = \phi_k(2\pi - \nu,\mu)$ for $k = i,o$, and $\phi_o(\nu,0) = 0$; this allows reducing the problem to finding the potential solution on the first quadrant only. Neglecting the contribution of the EDL to the external field as an approximation, we can expect that the fluid outside the EDL is electroneutral and of constant conductivity. Under these conditions, the electric potential distributions $\phi_k(\mu,\nu)$ are governed by Laplace's equation:

$$\nabla^2\phi_k = 0 \tag{S1}$$

where the Laplacian in elliptic coordinates takes the form

$$\nabla^2 = \frac{1}{a^2(\sinh^2\mu + \sin^2\nu)}\left(\frac{\partial^2}{\partial\mu^2} + \frac{\partial^2}{\partial\nu^2}\right) \tag{S2a}$$

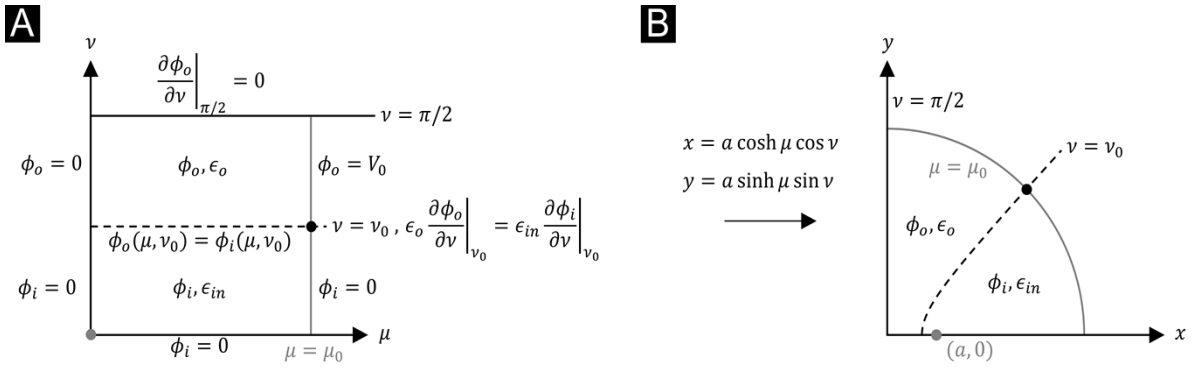

Fig. S1. Conformal mapping between rectangular and elliptic coordinates, for the first quadrant. A) Rectangular coordinates, with the corresponding boundary conditions for the electric potential inside ( ) and outside ( ) of the dielectric posts. B) Mapping to elliptic coordinates of system in A).

by introducing the mapping:

$$x = a\cosh\mu\cos\nu \tag{S2b}$$

$$y = a\sinh\mu\sin\nu\ . \tag{S2c}$$

The potential inside and outside the dielectrics can be obtained by mapping the first quadrant in rectangular coordinates to elliptic coordinates through eqns (S2b,c). Figure S1a,b illustrates this mapping, along with the boundary conditions in the mapped rectangular plane. Equation S1 is subject to the following boundary conditions:

$$\phi_o(\mu_0,\nu) = V_0\ ,\ \phi_i(\mu_0,\nu) = 0,\ \phi_k(0,\nu) = 0, \tag{S3a}$$

$$\left.\frac{\partial\phi_o}{\partial\nu}\right|_{\pi/2} = 0\ ,\ \phi_i(\mu,0) = 0, \tag{S3b}$$

$$\phi_i(\mu,\nu_0) = \phi_o(\mu,\nu_0), \tag{S3c}$$

$$\hat{n}\cdot(J_i - J_o) = \hat{n}\cdot(\sigma_i E_i - \sigma_o E_o) = 0, \tag{S3d}$$

where eqn (S3d) has been derived by applying the current continuity boundary condition between materials. Here, $\hat{n}$ is the interface unit normal vector, and J_k is the current density inside each material. Equation (S3d) can be rewritten in terms of the electric potential to find:

$$\left.\frac{\partial\phi_o}{\partial\nu}\right|_{\nu_0} = q\left.\frac{\partial\phi_i}{\partial\nu}\right|_{\nu_0}, \tag{S3e}$$

where $q = \sigma_i/\sigma_o$.

Because the Laplacian operator is separable in elliptic coordinates, we assume that eqn (S1) has non-trivial solutions of the form, $\phi_k = M_k(\mu)N_k(\nu)$, where $k = i,o$. The outer region is subject to non-homogeneous boundary conditions, and thus its solution can be separated into $\phi_o = \phi_{o,1} + \phi_{o,2}$ where $\phi_{o,1}$ is contingent on the homogeneous boundary value problem:

$$\phi_{o,1}(\mu_0,\nu) = V_0\ ,\ \phi_{o,1}(0,\nu) = 0 \tag{S4a}$$

$$\left.\frac{\partial\phi_{o,1}}{\partial\nu}\right|_{\pi/2} = \left.\frac{\partial\phi_{o,1}}{\partial\nu}\right|_{\nu_0} = 0\ . \tag{S4b}$$

It can be shown that eqn (S1) subject to conditions (S4a,b) can be generally solved by a function of the form $A\mu + B$, with $B = 0$, and $A = V_0/\mu_0$. The full solution on the outside is thus required to have the form:

$$\phi_o = \phi_{o,2} + \frac{\mu}{\mu_0} V_0$$

With the $\phi_{o,1}(\mu_0,\nu) = V_0$ condition taken care of, the potential $\phi_{o,2}$ can be found by setting the source V_0 to zero:

$$\phi_{o,2}(\mu_0,\nu) = 0 \ , \ \phi_{o,2}(0,\nu) = 0, \tag{S5a}$$

$$\left.\frac{\partial \phi_o}{\partial \nu}\right|_{\pi/2} = 0 \ , \tag{S5b}$$

Since solutions to $\phi_{o,2}$ have the separable form $\phi_{o,2}(\mu,\nu) = M(\mu)N(\nu)$, we find after examination of the eigenvalues that:

$$M(\mu) = c_1 \cos(\alpha\mu) + c_2 \sin(\alpha\mu) \tag{S6a}$$

$$N(\nu) = c_3 \exp(\alpha\nu) + c_4 \exp(-\alpha\nu) \tag{S6b}$$

where application of condition (S5a) leads to $c_1 = 0$, and the quantization of eigenvalues α:

$$\alpha\mu_0 = m\pi \Rightarrow \alpha = \frac{m\pi}{\mu_0}, \ m \in Z \ . \tag{S7}$$

Using condition (S5b) we eliminate one of the coefficients in eqn (S6b), so that $N(\nu) = c_4[\exp \alpha(\nu - \pi) + \exp(-\alpha\nu)]$. The superposition principle states that a solution can be constructed from the sum of all eigenfunctions:

$$\phi_{o,2}(\mu,\nu) = \sum_{m=1}^{\infty} A_m \left[\exp \frac{m\pi}{\mu_0}(\nu - \pi) + \exp -\frac{m\pi}{\mu_0}\nu\right] \sin\left(\frac{\mu\pi m}{\mu_0}\right) \tag{S8}$$

where coefficients c_1 and c_4 have been absorbed in the coefficient A_m, and the infinite sum is taken from $m = 1$ onwards (as the zero value leads to a trivial zero solution). Thus, the complete outside of the dielectric has the form:

$$\phi_o(\mu,\nu) = \sum_{m=1}^{\infty} A_m \left[\exp \frac{m\pi}{\mu_0}(\nu - \pi) + \exp -\frac{m\pi}{\mu_0}\nu \right] \sin\left(\frac{\mu\pi m}{\mu_0}\right) + \frac{\mu}{\mu_0} V_0 \quad \text{(S8)}$$

By similar arguments, it can be shown that the potential inside of the dielectric has the form:

$$\phi_i(\mu,\nu) = \sum_{m=1}^{\infty} B_m \sinh\left(\frac{m\pi\nu}{\mu_0}\right) \sin\left(\frac{\mu\pi m}{\mu_0}\right) \quad \text{(S9)}$$

which is not subject to inhomogeneous boundary conditions. To obtain the potentials inside and outside of the dielectric, it suffices to apply the interface boundary conditions (S3c,e) to eqns (S8) and (S9) to determine the coefficients A_m and B_m. Solving the resulting systems of equations leads to:

$$A_m = \frac{(-1)^m \left(1 + e^{\frac{2m\pi\nu_0}{\mu_0}}\right) q\, V_0}{m\pi \left(\frac{1}{2} e^{\frac{m\pi(\nu_0 - \pi)}{\mu_0}} \left(1 + e^{\frac{2m\pi\nu_0}{\mu_0}}(-1+q) + q\right) + q\cosh\left(\frac{m\pi\nu_0}{\mu_0}\right) + \sinh\left(\frac{m\pi\nu_0}{\mu_0}\right)\right)} \quad \text{(S10)}$$

$$B_m = \frac{2(-1)^m \left(-1 + e^{\frac{m\pi(2\nu_0 - \pi)}{\mu_0}}\right) V_0}{m\pi \left(\frac{1}{2} e^{\frac{m\pi(\nu_0 - \pi)}{\mu_0}} \left(1 + e^{\frac{2m\pi\nu_0}{\mu_0}}(-1+q) + q\right) + q\cosh\left(\frac{m\pi\nu_0}{\mu_0}\right) + \sinh\left(\frac{m\pi\nu_0}{\mu_0}\right)\right)} \quad \text{(S11)}$$

The outside and inside potentials thereby read:

$$\phi_o(\mu,\nu) = \sum_{m=1}^{\infty} \frac{(-1)^m \left(1 + e^{\frac{2m\pi\nu_0}{\mu_0}}\right) q\, V_0 \left(e^{\frac{m\pi}{\mu_0}(\nu - \pi)} + e^{-\frac{m\pi}{\mu_0}\nu} \right) \sin\left(\frac{m\pi\mu}{\mu_0}\right)}{m\pi \left(\frac{1}{2} e^{\frac{m\pi(\nu_0 - \pi)}{\mu_0}} \left(1 + e^{\frac{2m\pi\nu_0}{\mu_0}}(-1+q) + q\right) + q\cosh\left(\frac{m\pi\nu_0}{\mu_0}\right) + \sinh\left(\frac{m\pi\nu_0}{\mu_0}\right)\right)} + \frac{\mu}{\mu_0} V_0 \quad \text{(S12)}$$

$$\phi_i(\mu,\nu) = \sum_{m=1}^{\infty} \frac{2(-1)^m\left(-1+e^{\frac{m\pi(2\nu_0-\pi)}{\mu_0}}\right)V_0 \sinh\left(\frac{m\pi\nu}{\mu_0}\right)\sin\left(\frac{m\pi\mu}{\mu_0}\right)}{m\pi\left(\frac{1}{2}e^{\frac{m\pi(\nu_0-\pi)}{\mu_0}}\left(1+e^{\frac{2m\pi\nu_0}{\mu_0}}(-1+q)+q\right)+q\cosh\left(\frac{m\pi\nu_0}{\mu_0}\right)+\sinh\left(\frac{m\pi\nu_0}{\mu_0}\right)\right)}. \quad \text{(S13)}$$

Equations (S12) and (S13) represent the exact solution to the problem in Fig. S1. Our interest lays in determining the analytic expressions for the electric field. Noting that in elliptic coordinates, the electric field can be found through the formula:

$$E_k(\mu,\nu) = -\frac{1}{h_\mu}\frac{\partial\phi_k}{\partial\mu}\hat{\mu} - \frac{1}{h_\nu}\frac{\partial\phi_k}{\partial\nu}\hat{\nu} \quad \text{(S14)}$$

where $\hat{\mu}$, $\hat{\nu}$ are the unit vectors in elliptic coordinates, with $h_\mu = h_\nu = a\sqrt{\sinh^2\mu + \sin^2\nu}$ as scale factors. In particular, we are interested in finding the nonuniform field along the y-axis ($x = 0$) outside of the dielectric ($k = o$), or equivalently, at $\nu = \pi/2$. Applying the derivatives in eqn (S14) to eqns (S12,13), and using the mappings in eqns (S2b,c), it can be shown after mathematical manipulation that the field along the y-axis for the triangular post geometry is:

$$E_t(0,y) = \frac{-E_0}{\Omega\mu_0\sqrt{1+\left(\frac{y}{a}\right)^2}}\left[1 + Re\left\{\sum_{m=1}^{\infty}\alpha_m\left(\frac{y}{a}+\sqrt{1+\left(\frac{y}{a}\right)^2}\right)^{\frac{im\pi}{\mu_0}}\right\}\right]\hat{j}, \quad \text{(S14)}$$

where the summation coefficients α_m are given by:

$$\alpha_m = \frac{4(-1)^{m+1}(1+g^{2m})h^{m/2}q\,(1-q)^{-1}}{g^{3m}+\left(\frac{h}{g}\right)^m-(g^m+(hg)^m)\left(\frac{1+q}{1-q}\right)},$$

with the geometric functions $g = \exp\left(\pi\nu_0\mu_0^{-1}\right)$, $h = \exp\left(\pi^2\mu_0^{-1}\right)$, and $\mu_0 = \ln\left(\Omega^{-1}+\sqrt{\Omega^{-2}+1}\right)$. Moreover, the quantity:

$$\Omega = 2a/L \quad \text{(S15)}$$

has been introduced, which denotes the ratio between the interfocal distance $2a$ and the length of the microdevice L. The subindex t in eqn (S14) has also been introduced to denote the solution for the triangular geometry.

1.2 Approximations of Amplification Factor scaling laws at limiting cases

In the calculation of the amplification factors for the circular posts geometry (eqn (9) in the main Manuscript), there appears an infinite sum term that precludes an intuitive interpretation of the scaling of the amplification factor $\Psi_c(\gamma,q)$ with the geometrical parameter γ (the gap to post ratio), for the simplified case $q = 0$. The objective of this section is to perform a series of approximations on eqn (9) of the main Manuscript to arrive at a simple and intuitive expression that shows the scaling of Ψ_c with the geometrical parameter γ. Concretely, we wish to simplify the term:

$$1 - 8 \cdot \sum_{m=1}^{\infty} \frac{m(-1)^m}{g(\gamma)^{2m} - 1} \tag{S16}$$

where:

$$g(\gamma) = 1 + \gamma + \sqrt{\gamma(\gamma + 2)}\,.$$

Here, $g(\gamma)$ contains the geometric information needed for calculating Ψ_c. Since the limit $\gamma \gg 1$ means posts are very far apart from each other, this translates into no amplification, and thus one intuitively expects $\Psi_c \to 1$ (as confirmed by direct evaluation in Fig. 3 in the main Manuscript). The limiting case of the opposite end, i.e., $\gamma \ll 1$, is not intuitively calculated. We begin by approximating the geometric term elevated to the m-th power in eqn (S16) by a Puiseux series centered at $\gamma = 0$:

$$(1 + \gamma + \sqrt{\gamma(\gamma + 2)})^2 = 1 + 4\gamma + 2\gamma^2 + 2\sqrt{\gamma(\gamma+2)} + 2\gamma \approx 1 + 2\sqrt{2\gamma} + 4\gamma + O(\gamma^{3/2})$$

Neglecting higher order terms, the summation then becomes:

$$1 - 8 \cdot \sum_{m=1}^{\infty} \frac{m(-1)^m}{(1 + 2\sqrt{2\gamma} + 4\gamma)^m - 1}\,.$$

The trinomial to the m-th power can again be approximated by a Puiseux series at $\gamma = 0$, and thus:

$(1+2\sqrt{2\gamma}+4\gamma)^m \approx 1+2\sqrt{2\gamma}m+4\gamma m^2+O(\gamma^{3/2})$

Neglecting higher order terms and inserting this expression into the summation gives:

$$1-8\cdot\sum_{m=1}^{\infty}\frac{m(-1)^m}{1+2\sqrt{2\gamma}m+4\gamma m^2-1}=1-4\cdot\sum_{m=1}^{\infty}\frac{(-1)^m}{\sqrt{2\gamma}+2\gamma m}.$$

Factorizing the term $1/\sqrt{2\gamma}$ out of the summation yields:

$$1-\frac{4}{\sqrt{2\gamma}}\cdot\sum_{m=1}^{\infty}\frac{(-1)^m}{1+\sqrt{2\gamma}m}.$$

At this point, we note that the summation resembles form of a Lerch transcendent:

$$\Phi(z,s,a)=\sum_{k=0}^{\infty}\frac{z^k}{(a+k)^s} \tag{S17}$$

which can be connected to the polygamma function through the following identity:

$$\sum_{k=0}^{\infty}\frac{(-1)^k}{zk+1}=\frac{\Phi(-1,1,z^{-1})}{z}=\frac{1}{2z}\left(\psi_0\left(\frac{z+1}{2z}\right)-\psi_0\left(\frac{1}{2z}\right)\right) \tag{S18}$$

where ψ_0 denotes the zeroth order polygamma function (or digamma function):

$$\psi_0(x)=\frac{d}{dx}\ln(\Gamma(x))=\frac{\Gamma'(x)}{\Gamma(x)}\sim\ln x-\frac{1}{2x}. \tag{S19}$$

Since the summation can be split into the first and the rest of the terms different from $k=0$, we write:

$$\sum_{k=0}^{\infty}\frac{(-1)^k}{zk+1}=1+\sum_{k=1}^{\infty}\frac{(-1)^k}{zk+1},$$

and thus:

$$1+\sum_{k=1}^{\infty}\frac{(-1)^k}{zk+1}=\frac{1}{2z}\left(\psi_0\left(\frac{z+1}{2z}\right)-\psi_0\left(\frac{1}{2z}\right)\right).$$

Substituting $z=\sqrt{2\gamma}$, and $k=m$, we find:

$$\sum_{m=1}^{\infty}\frac{(-1)^m}{\sqrt{2\gamma}m+1}=\frac{1}{2\sqrt{2\gamma}}\left(\psi_0\left(\frac{\sqrt{2\gamma}+1}{2\sqrt{2\gamma}}\right)-\psi_0\left(\frac{1}{2\sqrt{2\gamma}}\right)\right)-1 .$$

Replacing the above summation into our original equation yields:

$$1-\frac{4}{\sqrt{2\gamma}}\cdot\left(\frac{1}{2\sqrt{2\gamma}}\left(\psi_0\left(\frac{\sqrt{2\gamma}+1}{2\sqrt{2\gamma}}\right)-\psi_0\left(\frac{1}{2\sqrt{2\gamma}}\right)\right)-1\right)=$$

$$1+\frac{1}{\gamma}\left(\psi_0\left(\frac{1}{2\sqrt{2\gamma}}\right)-\psi_0\left(\frac{\sqrt{2\gamma}+1}{2\sqrt{2\gamma}}\right)\right)+\frac{4}{\sqrt{2\gamma}} .$$

Recalling the approximation for the digamma function in eqn (S19) simplifies the above equation into:

$$1-\frac{2}{1+\sqrt{2\gamma}}+2\sqrt{\frac{2}{\gamma}}+\frac{\ln\left(\frac{2}{\gamma}\right)-2\ln\left(2+\sqrt{\frac{2}{\gamma}}\right)}{2\gamma},$$

which to zeroth order approximation is equal to:

$$1-\frac{2}{1+\sqrt{2\gamma}}+2\sqrt{\frac{2}{\gamma}}+\frac{\ln\left(\frac{2}{\gamma}\right)-2\ln\left(2+\sqrt{\frac{2}{\gamma}}\right)}{2\gamma}\approx\sqrt{\frac{2}{\gamma}}+O(\gamma^{1/2}) .$$

Thus, the amplification factor at the origin for the bipolar coordinate system, assuming $q=0$ and $\gamma\ll 1$, scales as:

$$\Psi_c(\gamma)\sim\sqrt{\frac{2}{\gamma}}+O(\gamma^{1/2}) . \qquad \text{(S20)}$$

2 Computational model for the nonuniform electric field

2.1 3D Model Geometry for the E-Field Optimization

We illustrate the 3D Geometry used in the computational model to numerically compute the results presented in Fig. 4A-E. The amplification factors (Ψ_c^N and Ψ_t^N) plotted in Fig. 4A,B were obtained by extracting the amplification factor at $x = y = 0$ for both the circular and triangular 3D geometries (corresponding to the maximum amplification along a 10,000 μm cutline, shown in red in Fig S2A) On the other hand, the magnitude of the electric current density at the gap region (plotted in Fig. 4C,D) was numerically computed by dividing the electric flux $\phi_E = \int E \cdot d\mathbf{A}$ by the area of the constriction at different gap sizes—i.e., effectively averaging the electric field over the constriction area—and multiplying the resulting quantity by σ_m. Here, constriction area was defined as the product of the gap length by the device height ($G \cdot H$, with $H = 40$ μm), this is illustrated in Fig. S2B. The same procedure was followed to compute the magnitude of the average of the gradient of the electric field squared over the constriction area ($|\nabla(E \cdot E)|$, plotted in Fig. 4E) with the electric flux integral being replaced by $\Phi_{\nabla(E \cdot E)} = \int \nabla(E \cdot E) \cdot dA$.

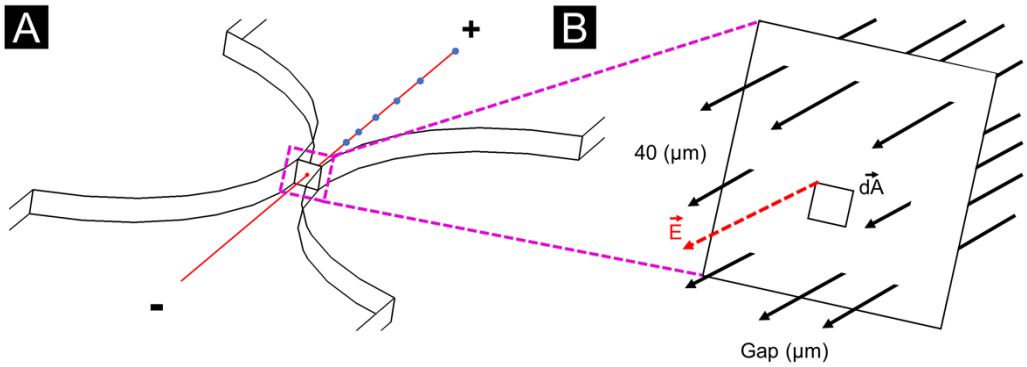

Fig. S2. Illustration of the 3D geometry used in the computational model. A) Illustration of the 10,000 μm cutline (red) extending across the length of the channel as well as a conceptual illustration of the displacement of an ideal particle (blue) moving from the positive to the negative electrode along the cutline. B) Illustration of the constriction area at x = y = 0 μm used for computing $|J|$ and $|\nabla(E \cdot E)|$.

Furthermore, the theoretical first trapping results are defined as the applied potential difference at which particles begin to trap (i.e., when there is a balance of the linear EO and EP phenomena and higher order effects of $EP^{(3)}$ for the buffer−particle−electric field system) at the gap between posts while other particles keep flowing through. The first trapping results presented in Fig. 5A,B and in Table 2 were calculated by means of eqn (6) in combination with the EK properties of Table 1 of the main Manuscript. For each particle and channel combination we computed the mean velocity (u_p) that an ideal particle like the one

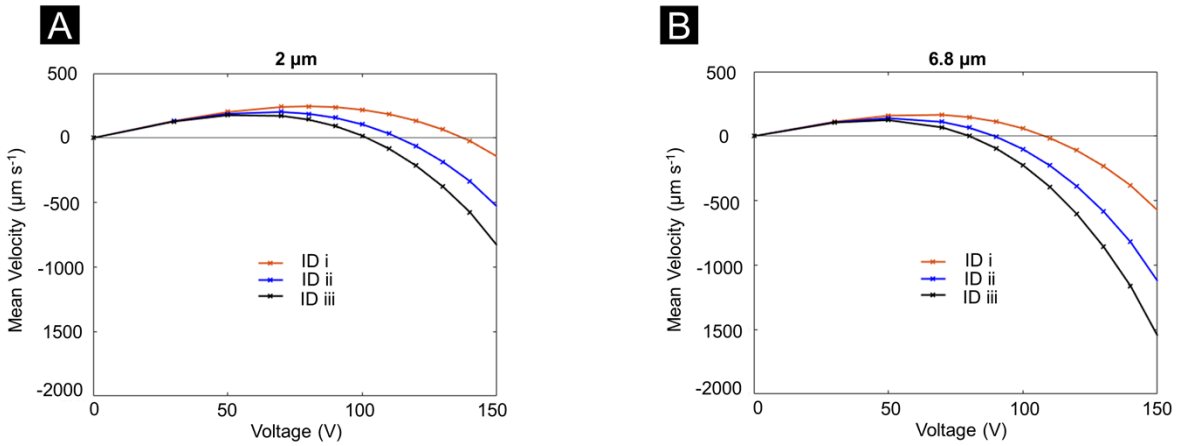

Fig. S3. Plots of the theoretical mean velocity that a particle would experience when travelling across a channel configuration at a given voltage. The intersection between the velocity curves and the horizontal line at u_p= 0 µm s^{-1} represents the voltage at which particles halt (i.e., zero velocity), the results are plotted for A) the 2 µm particle and B) the 6.8 µm particle.

shown in Fig. S2A would experience when travelling across the length of the channel while following the 10,000 μm cutline shown in red in Fig.S2A. This enabled us to simulate the mean velocity that a given particle would experience in a specific channel configuration at a given electric field magnitude and use this information to determine the theoretical electric field magnitude—and hence, voltage—at which particles halt (i.e., zero velocity), the results are plotted in Fig. S3A,B for the 2 and 6.8 μm particles, respectively. The average relative error between the experimental and theoretical first trapping for all cases is 18.02% with the relative error for the ideal geometry (ID iii) being of only 3.66%.

3 Table S1

Table S1. Conditions, definitions, and input data used in COMSOL models (see Figure 1 for more details).

Module	**Element (see Figure 1a)**	**Definition**
Current conservation	Blue and Gray	$\nabla \cdot J = Q_j;$ $J = \left(\sigma + \varepsilon_0 \varepsilon_r \frac{\partial}{\partial t}\right) E + J_e;\ E = -\nabla V$
Electric insulation	Channel edge	$n \cdot J = 0$
Initial values	Blue and Gray	$V_0 = 0$
Electric potential	Left electrode (+)	$\phi = \phi_{inlet}$
Ground	Right electrode (-)	$\phi = 0$

*In this table, J is the electric current, $Q_j = -\frac{d\rho_v}{dt}$ (where ρ_v represents the volume charge density), J_e is an external electric current density.

4 Table S2

Table S2. Input and mesh parameters used for COMSOL simulations.

Parameter	Value	Units
*Electric conductivity of the medium, σ_o	25	[µS/cm]
Permittivity of medium, ϵ_o	80.00	[adim.]
Electric conductivity of the PDMS, σ_i	2.5E-8	[µS/m]
Permittivity of PDMS, ϵ_i	2.75	[adim.]
Type of mesh elements	Tetrahedral	N/A

* Measured experimentally in our laboratory.

5 Video S1: Fluorescent analysis

The fluorescence intensity data (background subtracted) near the constriction versus time (i.e., the applied voltage) were fitted into two segments, whose intersection point was taken as a variable optimized using the least squares method by a customized MATLAB R2018b (Mathworks Inc., Natick, MA) code. The applied voltage corresponding to the determined intersection point between the segments was extracted as the total trapping voltage (See Table 2). This enables an automatic and objective determination of the trapping voltage. All experiments were run in triplicate to ensure reproducibility. We found that we could increase the accuracy of our total trapping determination method by defining two regions of interest (ROI), one on the left and one on the right of the constriction; this reduced the average standard deviation between trials from ± 31.27 V to ± 23.35 V. We then determined the background intensity for each voltage as the difference between the average fluorescence level prior to the first trapping voltage (shown in Table 2) and the intensity at the region located after the posts, further reducing the average standard deviation between trials to ± 18.46 V. A possible explanation for the effectiveness of this method is that prior to first trapping, particles are still crossing the channel and contributing to the overall intensity level, so by subtracting the average background intensity of the particles flowing across the channel, we registered an increase in fluorescence when particles truly begin trapping. The S1 video demonstrates the implementation of this method, with the top left corner showing one trial with the 6.8 μm particle in the ID iii device shown in Fig. 1B iii of the main text, the bottom showing the fluorescence intensity graph as the experiment progresses, and the top right corner showing the slope difference between datapoints

allowing for the determination of the best intersection point between two piecewise segments adjusting the data.